Fractals, Vol. 18, No. 1 (2010) 127–138

DOI: 10.1142/S0218348X10004749

World Scientific
www.worldscientific.com

EFFECTS OF BIT DEPTH ON THE MULTIFRACTAL ANALYSIS OF GRAYSCALE IMAGES

H. ZHOU,*,† E. PERFECT,† B. G. LI* and Y. Z. LU*,‡
*Department of Soil and Water Sciences
China Agricultural University
Beijing, 100193, P. R. China
†Department of Earth and Planetary Sciences
University of Tennessee, Knoxville, TN 37996-1410, USA
‡lyz@cau.edu.cn

Received March 23, 2009
Accepted September 28, 2009

Abstract

Multifractal box counting analysis has been widely applied to study the scaling characteristics of grayscale images. Since bit depth is an important property of such images it is desirable know the impact of varying bit depths on the estimation of the generalized dimensions (D_q). We generated random geometrical multifractal grayscale fields, which were then transformed from double precision to 16, 13, and 8 bit depths. Digitized grayscale images of soil thin sections at 13 bit depth were also selected for study and transformed to 8 bit depth. The moment based box counting method was applied to evaluate the bit depth effects on D_q. The partition functions for the multifractal fields became noticeably nonlinear on a log-log scale when $q \ll 0$ as the bit depth decreased. This trend can be attributed to loss of grayscale details, changes in the local mass distribution, and the occurrence of zeros due to the bit depth transformation and data normalization processes. These effects were most pronounced for positively skewed multifractal fields, with a high proportion of extremely small mass fractions. As a result, the generalized dimensions estimated by linear regression were not always accurate, and an alternative method based on numerical derivatives was explored. The numerical method significantly improved the accuracy of the multifractal analyses; the maximum absolute difference between the analytical and numerically-derived estimates of D_q was only 9.62×10^{-3}. However, when

‡Corresponding author.

applied to situations in which the box counting scale factor did not match the scale factor used to generate the multifractal field, the numerically-derived estimates of D_q were severely biased. In this case, the linear regression method is preferable even though some error may occur due to limited bit depths. All of the soil grayscale images exhibited multifractal scaling characteristics, although there was little effect of bit depth on the resulting D_q values. Because of random fluctuations in the partition functions, the linear regression method proved to be more robust than the numerical derivative method for estimating the generalized dimensions of natural grayscale images.

Keywords: Bit Depth; Generalized Dimensions; Image Analysis; Multifractal; Grayscale Fields; Method of Moments; Soil Thin Section.

1. INTRODUCTION

Multifractal box counting analysis is a powerful quantitative technique for characterizing the scaling behavior of heterogeneous data sets. Both spatial and temporal data can be analyzed using this approach. As a result, it has been employed in a wide variety of disciplines including, for example, remote sensing,[1] medical diagnoses,[2] soil science,[3] and material science.[4] In the spatial domain, multifractal box counting analyses are commonly performed on grayscale digital images, including X-ray medical images,[5] satellite imagery,[1] scanning electron microscopy (SEM) images[6] and other optical images. With such analyses, the accuracy of the estimated multifractal parameters relies upon the quality of the digital images.

Bit depth, which refers to the number of colors available to each pixel in a color image or the number of shades available in a grayscale image, is an important property of digital images.[7] This paper deals with grayscale images. The most common format for such images is 8 bit depth, meaning that a total of $2^8 = 256$ grayscales are available to each pixel. Although this number may be sufficient for the naked eye, the details of heterogeneous images may be lost because of the limited number of shades of gray. Digital images of more than 8 bit depth are available nowadays, and the increased bit depth provides more shades of gray. However, the increase in bit depth sharply increases the file size of the image, and thus the computer processing time required. To choose an appropriate digital image format for analysis, it is important to know the effects of bit depth on the estimation of multifractal parameters.

The generalized dimensions (D_q) are commonly used to parameterize multifractal scaling.[8] However, it's not easy to calculate D_q because of the limited resolution of digital images.[3] The method of moments,[9,10] which is based on the box counting method, is a practical method to compute D_q, and has been widely employed in a variety of studies. This method uses linear regression analysis to estimate D_q from the slope of the log-log transformed partition function, $\chi(q, \delta)$. When analyzing normalized grayscale fields, with pixel values ranging between zero and unity, the regression method has been shown to overestimate D_q.[11] For such fields, the numerical differentiation method proposed by Perfect *et al.*[11] provides more accurate results than linear regression analysis.

To our knowledge, no studies have previously evaluated the effects of bit depth on the multifractal analysis of grayscale images. In this paper we first demonstrate the influence of bit depth on D_q estimated from geometrical multifractals and natural images. We then investigate the improvement in accuracy obtained with the numerical differentiation method. Finally, we show how D_q can be influenced by the choice of the box counting scale factor.

2. METHODS

2.1. Random Geometrical Multifractals

Random geometrical multifractals were constructed according to the algorithm of Perfect *et al.*[11] An initiator of unit length was divided into a grid of b^2 cells, where b is an integer scale factor > 1. Mass fractions, μ_{j_1}, were computed for the $j_1 = 1$ to b^2 cells of the grid according to the formula:

$$\mu_{j_1} = \sum_{j_1=1}^{b^2} B_T(j_1, b^2, p)\frac{1}{j_1}, \qquad (1)$$

where $B_T(j_1, b^2, p) = \binom{b^2}{j_1} p^{j_1}(1-p)^{b^2-j_1} / \sum_{j_1}^{b^2} \times \binom{b^2}{j_1} p^{j_1}(1-p)^{b^2-j_1}$ is the truncated binomial probability[12] for getting j_1 "successes" in a b^2 grid when the selected probability is p, and $\binom{b^2}{j_1}$ is the binomial coefficient. The resulting mass fractions were then randomly assigned to the b^2 cells of the first iteration ($i = 1$) grid or generator.

The generator was applied onto itself by repeating the above process for each of b^2 cells in the $i = 1$ grid. Thus, at $i = 2$ the grid contained $j_2 = 1$ to $(b^2)^2$ cells. The values of the corresponding mass fractions were calculated as:

$$\mu_{j_2} = \mu_{j_1} \times \mu_{j_1} \tag{2}$$

and randomly assigned to those cells within the $i = 1$ subunits of the grid. Repetition of this multiplicative cascade to the ith iteration level produces a random multifractal Sierpinski carpet.

2.2. Analytical Generalized Dimensions

Analytical generalized dimensions for the random multifractal Sierpinski carpets were computed according to Perfect *et al.*[11]:

$$D_q = \frac{1}{q-1} \log \left(\left(\sum_{j_1}^{b^2} (\mu_{j_1})^q \right)^{-1} \right) \Big/ \log(b); \quad q \neq 1 \tag{3}$$

where D_q is the Rényi or qth order generalized dimension, and q is any integer value between $\pm\infty$. When $q = 1$, the following expression was used:

$$D_1 = -\sum_{j=1}^{b^2} \mu_{j_1} \times \log(\mu_{j_1}) / \log(b), \tag{4}$$

where D_1 is the information or entropy dimension.

2.3. Multifractal Grayscale Fields

Grayscale fields were created from the random multifractal Sierpinski carpets by normalizing the mass fractions at the ith iteration level using the expression: $g_{j_i} = \frac{\mu_{j_i} - \mu_{\min}}{\mu_{\max} - \mu_{\min}}$, where $\mu_{\max} = (\mu_1)^i$ and $\mu_{\min} = (\mu_{b^2})^i$ are the maximum and minimum mass fractions at the ith iteration level, respectively. As is usually done in digital image processing, the extreme values in each field, i.e., $g_{j_i} = 0$ and 1, were represented visually by black and white, respectively.

In this study, three random multifractal grayscale (RMG) fields, each containing $(b^i)^2 = 1024 \times 1024$ cells were constructed by selecting $b = 4$ and $p = 13, 14$ or 15 in Eq. (1), and iterating the generator $i = 5$ times. It is important to note that each cell of each field contains a different value of g_{j_i} (i.e., 20 bits). All the fields were stored in IEEE standard double precision (64 bits), which was more than sufficient to accommodate all of the grayscale values present. The resulting high resolution grayscale fields are shown in Figs. 1(a)–1(c).

Lower resolution RMG fields were obtained by degrading the grayscale values in the high resolution fields to 16, 13 and 8 bit depths, respectively. These transformations were performed in Matlab 7.0 using the formula: round $(g_{j_i} \times (2^{\text{bit}} - 1))/(2^{\text{bit}} - 1)$, where "round" is a function that rounds the number in parentheses to the nearest integer, and bit = 16, 13 or 8 depending upon the desired resolution. Thus, although the fields all contain the same number of cells, there is a progressive reduction in the number of grayscale values represented. Selected statistical properties of the 12 RMG fields (3 p values $\times$ 4 bit depths) are listed in Table 1.

2.4. Soil Thin Section Images

Undisturbed soil samples were obtained from the long-term tillage experiment station of Jilin Academy of Agricultural Sciences (42°57′N, 148°57′E), Gongzhuling City, Jilin Province, China. Soil thin sections of 0.03 mm thickness were then made following the methods described in Murphy.[13] Digital grayscale images of the soil thin sections were acquired at 13 bit depth under the same light intensity with a Nikon DS-Fi1 digital camera equipped on a Nikon Eclipse Lv100Pol polarized microscope. The dimensions of the resulting images were 2560 × 1920 pixels, with a pixel length of 1.9 μm. To avoid edge effects, and to be consistent with the RMG fields, the central part of each image was cropped to 1024 × 1024 pixels. The raw pixel values were normalized to give grayscale values between zero (black) and one (white).

Three soil thin section (STS) images showing different structural characteristics were selected for detailed study (see Figs. 1(d)–1(f)). A lower resolution version of each 13 bit depth image was obtained by rounding to 8 bit depth using the same procedure used to transform the RMG fields (see Sec. 2.3). The statistical moments of the six STS images (three soils × two bit depths) are given in Table 1.

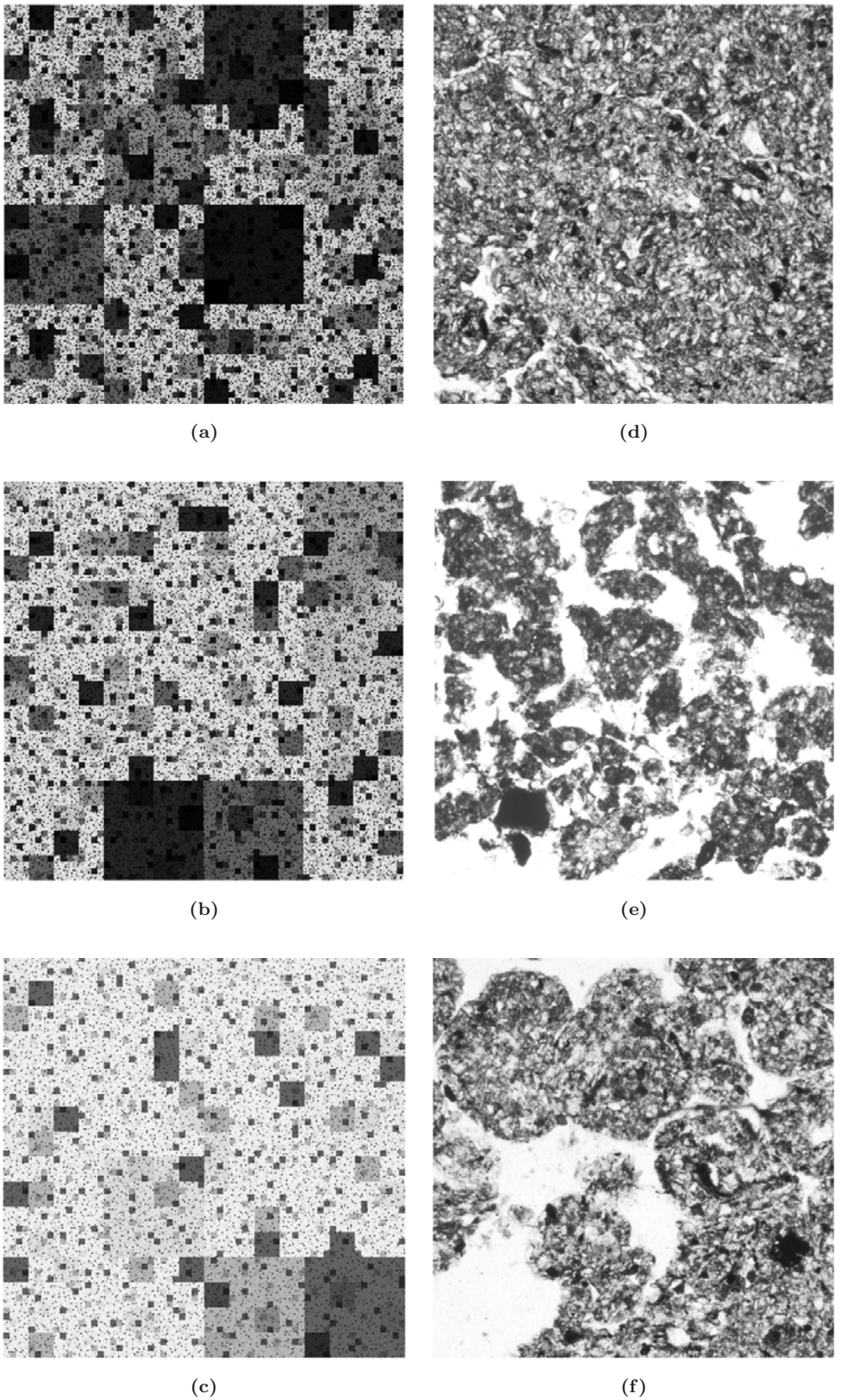

Fig. 1 Six grayscale images of size 1024×1024 pixels: **(a)** RMG#1, generated with $b = 4$, $p = 13/16$, and $i = 5$; **(b)** RMG#2, generated with $b = 4$, $p = 14/16$, and $i = 5$; **(c)** RMG#3, generated with $b = 4$, $p = 15/16$, and $i = 5$; **(d)** STS#1; **(e)** STS#2; and **(f)** STS#3.

Table 1 Grayscale Fields and Their Statistical Properties.

Field Type	Field #	Bit Depth	First Moment	Second Central Moment	Third Central Moment	Forth Central Moment
RMG	1	DP	0.327	1.26×10^5	3.36×10^4	3.15×10^4
RMG	2	DP	0.489	1.38×10^5	6.55×10^3	2.61×10^4
RMG	3	DP	0.707	9.48×10^4	-1.73×10^4	1.58×10^4
RMG	1	16	0.327	1.26×10^5	3.36×10^4	3.15×10^4
RMG	2	16	0.489	1.38×10^5	6.55×10^3	2.61×10^4
RMG	3	16	0.707	9.48×10^4	-1.73×10^4	1.58×10^4
RMG	1	13	0.327	1.26×10^5	3.36×10^4	3.15×10^4
RMG	2	13	0.489	1.38×10^5	6.55×10^3	2.61×10^4
RMG	3	13	0.707	9.48×10^4	-1.73×10^4	1.58×10^4
RMG	1	8	0.327	1.27×10^5	3.36×10^4	3.16×10^4
RMG	2	8	0.489	1.37×10^5	6.56×10^3	2.60×10^4
RMG	3	8	0.707	9.48×10^4	-1.74×10^4	1.58×10^4
STS	1	13	0.326	2.30×10^5	8.01×10^4	7.85×10^4
STS	2	13	0.485	2.62×10^5	7.74×10^3	6.57×10^4
STS	3	13	0.695	2.22×10^5	-8.67×10^4	8.09×10^4
STS	1	8	0.460	5.49×10^4	5.13×10^3	6.42×10^3
STS	2	8	0.517	1.20×10^5	6.10×10^3	1.92×10^4
STS	3	8	0.591	8.30×10^4	-1.86×10^3	1.11×10^4

Note: RMG = multifractal grayscale field, STS = soil thin section image, DP = double precision; RMG #1, #2 and #3 constructed using $b = 4$, $i = 5$, and $p = 13/16$, $p = 14/16$ and $p = 5/16$, respectively.

2.5. Empirical Generalized Dimensions

The method of moments was used to estimate empirical generalized dimensions for the RMG fields and STS images. Since the theory behind this box counting method has been described by other authors,[9,10] the calculation procedures are only briefly outlined here. The normalized grayscale values, g_{j_i}, were converted to probability density values, ρ_{j_i}, using the relationship $\rho_{j_i} = g_{j_i}/\sum_{j_i=1}^{b^{2i}} g_{j_i}$ The resulting probability density fields were then subdivided into square grids with variable box lengths, $\delta = \beta^j$, where β is the box counting scale factor, and j is an integer value between zero and $\log_\beta(b^i)$. In this study, β was set to either 4 (i.e., $\beta = b$) or 2 (i.e. $\beta \neq b$), with $0 \leq j \leq \log_\beta(1024)$.

The probability density value of the kth box in a superimposed grid, $\rho_k(\delta)$, was calculated as the sum of all the probability density values within that box. A weighted summation performed over all the boxes in a particular grid yielded the partition function of order q, i.e.

$$\chi(q,\delta) = \sum_{k=1}^{\delta^{-2}} (\rho_k(\delta))^q. \tag{5}$$

For a multifractal field, this partition function scales with the box length as:

$$\chi(q,\delta) \propto \delta^{-\tau(q)}, \tag{6}$$

where $\tau(q)$ is the mass exponent for q. Taking the logarithms of both sides of Eq. (6), linear regression analysis was used to estimate $\tau(q)$ from the slope of the best-fit line. The generalized dimensions, D_q, were then calculated from $\tau(q)$ using the relationship:

$$D_q = \frac{\tau(q)}{q-1}. \tag{7}$$

For $q = 1, D_1$ was estimated directly from the slope of a linear regression analysis performed on $\sum_{k=1}^{\delta^{-2}} \rho_k(\delta)\log(\rho_k(\delta))$ versus $\log(\delta)$. This method for computing the empirical generalized dimensions will hereafter be referred to as the linear regression method.

Perfect *et al.*[11] proposed an alternative method to estimate $\tau(q)$ based on the following three point formula for an end point numerical derivative:

$$y'(x) = \frac{-3y(x) + 4y(x+h) - y(x+2h)}{2h}, \tag{8}$$

where $y = \log(\chi(q,\delta))$, $x = \log(\delta)$, and h is a finite difference corresponding to $\log(\beta^j) - \log(\beta^{j-1})$ as $j \to \log_\beta(b^i)$. This numerical method was shown

to improve the accuracy of empirical generalized dimensions estimated from normalized multifractal grayscale fields. Therefore, it was also included in the present study, and will subsequently be referred to as the numerical derivative method.

3. RESULTS AND DISCUSSION

3.1. Statistical Properties of the Grayscale Fields

The statistical properties of the grayscale fields were first examined in order to better understand differences in the empirical multifractal analyses. Bit depth had little effect on the moments of the RMG fields (Table 1). Mean whiteness (as quantified by the first moment of the g_{j_i} values) progressively increased as the p value used to generate the RMG fields increased (Figs. 1(a)–1(c), Table 1). Histograms of the g_{j_i} values for the 13 bit depth fields indicated very jagged, discrete frequency distributions (Figs. 2(a)–2(c)). As the p value increased, there was a corresponding increase in the frequency of g_{j_i} values close to unity, and a concomitant decrease in the frequency of g_{j_i} values close to zero. The third central moment, which characterizes the skewness of a distribution, indicated a pronounced shift from positive to negative skew as the p value increased from 13/16 to 15/16 (Table 1).

As indicated by the first moments in Table 1, the three STS images selected for study also exhibited marked differences in mean whiteness. Furthermore, the third central moments of the STS images showed a similar shift from positive to negative skew with increasing mean whiteness. The higher order moments for the STS images were generally more sensitive to bit depth than was the case for the RMG fields (Table 1). The histograms of the g_{j_i} values for the three STS images (Figs. 2(d)–2(f)) were much smoother and continuous compared to the frequency distributions for the RMG fields (Figs. 2(a)–2(c)).

3.2. Generalized Dimensions Estimated by the Linear Regression Method

Selected log-log plots of the partition function versus box size for the RMG and STS fields are illustrated in Fig. 3. When $q \gg 0$, the $\log(\chi(q,\delta))$ versus $\log(\delta)$ relations were always linear regardless of the bit depth or image type, hence these results were not included in Fig. 3.

Compared with the analytical relationship, a distinct underestimation of $\chi(q, \delta)$ occurred with the empirical results for RMG #1 when $q \ll 0$ (Fig. 3(a)). This underestimation was most

Table 2 Summary of Empirical Multifractal Analyses with $\beta = 2$ and $\beta = 4$.

Field	Bit Depth	$R^2(q=-10)$		$D_{q=-10}$		ΔD_q		$D_{q=1}$		$D_{q=2}$	
		$\beta=2$	$\beta=4$	$\beta=2$	$\beta=4$	$\beta=2$	$\beta=4$	$\beta=2$	$\beta=4$	$\beta=2$	$\beta=4$
RMG#1	DP	0.994	0.998	3.93	3.89	2.08	2.03	1.91	1.92	1.89	1.89
RMG#2	DP	0.997	0.999	3.20	3.16	1.29	1.25	1.95	1.95	1.94	1.94
RMG#3	DP	0.999	0.999	2.54	2.52	0.58	0.56	1.98	1.98	1.98	1.98
RMG#1	16	0.981	0.979	3.45	3.29	1.59	1.43	1.91	1.92	1.89	1.89
RMG#2	16	0.996	0.998	3.19	3.15	1.28	1.24	1.95	1.95	1.94	1.94
RMG#3	16	0.999	0.999	2.54	2.52	0.58	0.56	1.98	1.98	1.98	1.98
RMG#1	13	0.974	0.973	3.12	2.97	1.27	1.12	1.91	1.92	1.89	1.89
RMG#2	13	0.995	0.995	3.11	3.03	1.20	1.12	1.95	1.95	1.94	1.94
RMG#3	13	0.999	0.999	2.54	2.52	0.58	0.56	1.98	1.98	1.98	1.98
RMG#1	8	0.963	0.970	2.58	2.46	0.73	0.60	1.91	1.92	1.89	1.89
RMG#2	8	0.986	0.987	2.64	2.56	0.73	0.65	1.95	1.95	1.94	1.94
RMG#3	8	0.999	0.999	2.55	2.54	0.59	0.58	1.98	1.98	1.98	1.98
STS#1	13	0.997	0.997	2.33	2.31	0.42	0.40	1.98	1.98	1.96	1.96
STS#2	13	0.994	0.995	2.36	2.33	0.45	0.42	1.96	1.96	1.94	1.94
STS#3	13	0.995	0.996	2.37	2.35	0.42	0.40	1.98	1.98	1.97	1.97
STS#1	8	0.997	0.997	2.33	2.31	0.42	0.40	1.98	1.98	1.96	1.96
STS#2	8	0.994	0.995	2.36	2.34	0.45	0.42	1.96	1.96	1.94	1.94
STS#3	8	0.995	0.999	2.37	2.35	0.42	0.40	1.98	1.98	1.97	1.97

Note: RMG = multifractal grayscale field, STS = soil thin section image, DP = double precision; $\Delta D_q = D_{q=-10} - D_{q=10}$.

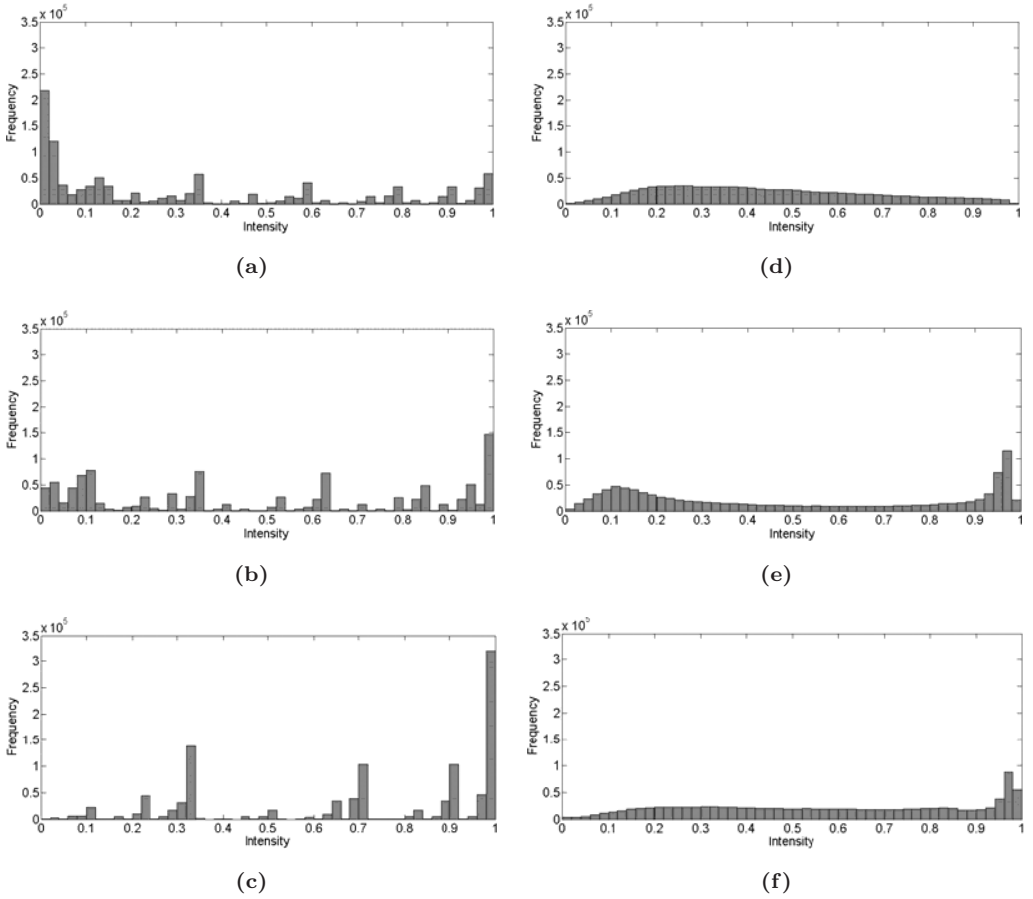

Fig. 2 Histograms of the 13 bit depth grayscale fields: **(a)** RMG#1; **(b)** RMG#2; **(c)** RMG#3; **(d)** STS#1; **(e)** STS#2; and **(f)** STS#3.

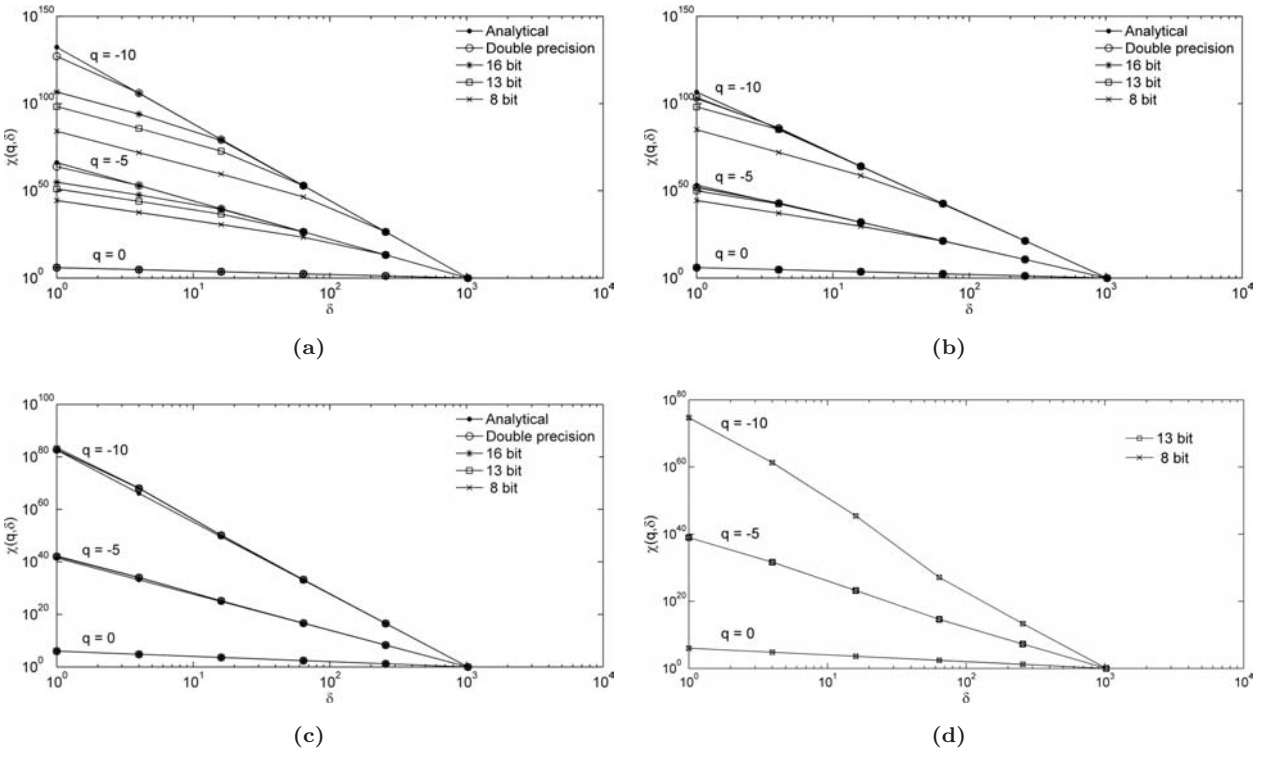

Fig. 3 Influence of different bit depths on the partition functions at $q = -10$, -5 and 0 for: **(a)** RMG#1; **(b)** RMG#2; **(c)** RMG#3; and **(d)** STS#1.

pronounced as $\delta \rightarrow 1$, and increased as the bit depth decreased. The $\log(\chi(q,\delta))$ versus $\log(\delta)$ relations clearly deviate from linearity. Similar, albeit less pronounced, trends were observed in the case of RMG #2 (Fig. 3(b)). Only slight deviations were observed for RMG #3 (Fig. 3(c)), although the $\chi(q, \delta)$ was overestimated at limited bit depths.

In this study, only 13 and 8 bit depth images were available for the soil thin sections, and of course no analytical functions were available for these fields. Unlike the multifractal grayscale fields, virtually no differences in $\chi(q, \delta)$ were observed between the 13 and 8 bit depth STS images when $q \ll 0$. Since all three soils behaved similarly, only a single example is shown in Fig. 3(d).

The results of the linear regression method applied to the $\log(\chi(q,\delta))$ versus $\log(\delta)$ relations are summarized in Table 2. Despite nonlinearities in the log-transformed partition functions for some of the RMG fields, coefficients of determination (R^2) from the regression analyses were always ≥ 0.97 when $\beta = b$. The R^2 values for the STS images were always ≥ 0.99 regardless of bit depth or β value. This result, coupled with the observation that $\Delta D_q > 0.40$, suggests that these natural images can be considered, at least in a statistical sense, random multifractal grayscale fields.

Generalized dimensions calculated from the slopes of the linear regression analyses showed similar trends to those observed with $\chi(q, \delta)$ (Fig. 4). For the multifractal fields, decreasing bit depth biased the estimates of D_q as q became increasingly negative (Figs. 4(a)–4(c)). The greatest effect of bit depth on D_q was observed with the RMG #1 field. It is important to point out that the impact of bit depth of the estimation of D_q appears to be much greater than the normalization effect reported by Perfect *et al.*[11] The bias introduced by normalization can be seen by comparing the double precision results with the analytical values in Figs. 4(a)–4(c).

While bit depth had a significant effect on the estimation of generalized dimensions for RMG fields with low p values, estimates of D_q for the natural grayscale images were almost the same for the 13 and 8 bit depths (Fig. 4(d)). Root mean squared errors (RMSE's) between the 13 and 8 bit depth soil images (computed over the range $q = -10$ to $+10$) were 4.0×10^{-5}, 4.6×10^{-4} and 2.6×10^{-4} for STS #1, #2 and #3, respectively. In contrast,

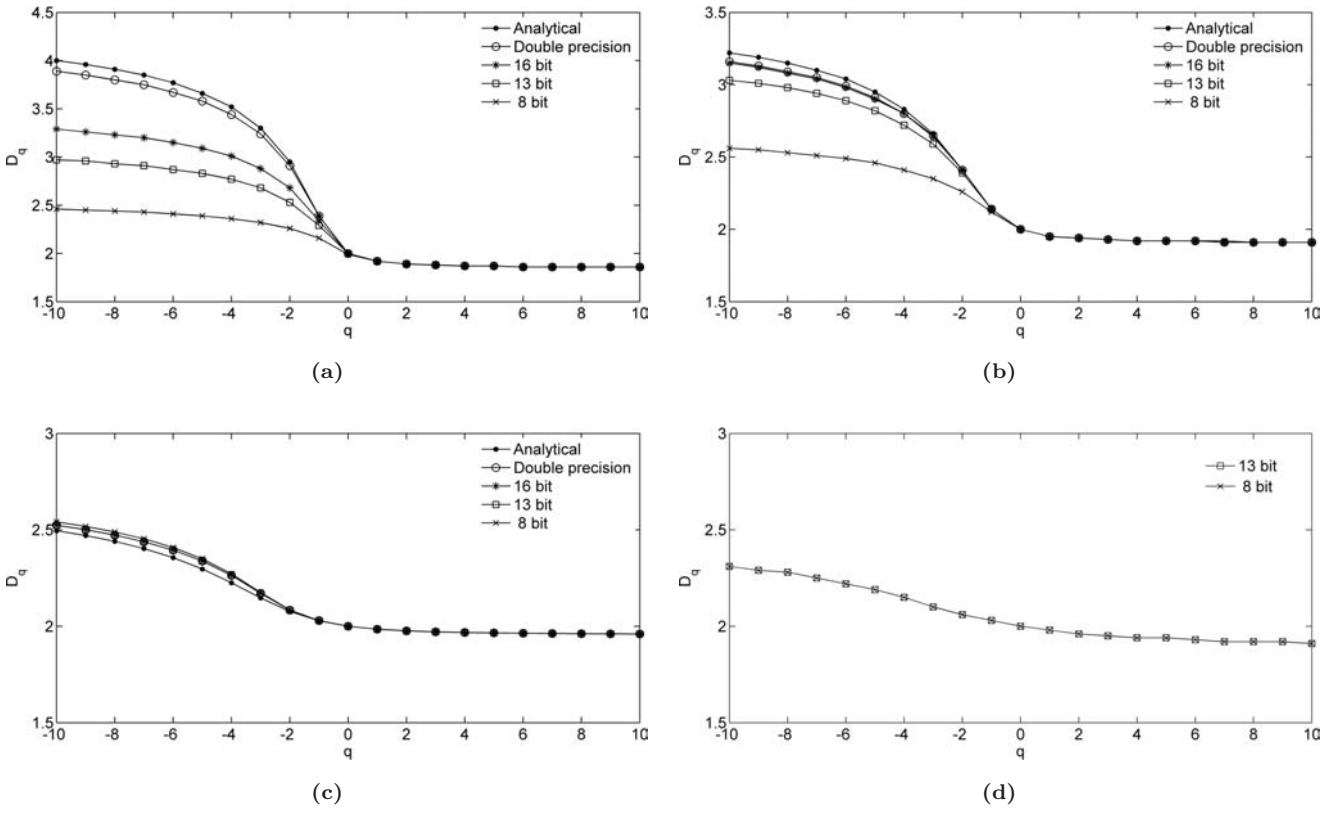

Fig. 4 Influence of different bit depths on the generalized dimensions at $q = -10$ to $+10$ for: **(a)** MF#1; **(b)** MF#2; **(c)** MF#3; and **(d)** Soil#1.

corresponding RMSE's between the 13 and 8 bit depth multifractal fields were 0.29, 0.25 and 0.08 for RMG #1, #2 and #3, respectively.

Given the above observations, it is logical to ask the following questions: (1) what is the underlying cause of the bit depth effect, and (2) why does it impact the multifractal and natural grayscale fields differently? Processing the different RMG fields involves the transformation of data from double precision to more limited bit depths, as well as the normalization of data to between zero and one. Perfect *et al.*[11] have already examined the effects of normalization on the estimation of D_q. In the present study, the deviations of the partition functions for the double precision RMG fields were caused solely by this normalization process. It is apparent from Figs. 3 and 4, however, that deviations in D_q due to limited bit depth can be much more pronounced.

The bit depth effect can be attributed to several interrelated factors. First, during the transformation of the data for the RMG fields from double precision to limited bit depths, several grayscales were binned together into a single value (e.g., 32 shades were binned into one shade when images of 13 bit depth were transformed to 8 bit depth). As a result the finer details of these shades were lost. Additionally, because of the heterogeneous nature of the spatial distributions, the rounding process can alter the local mass distribution. For example, the total mass fraction for the 4×4 pixels in the upper left corner of RMG #1 was 2.22859×10^{-5} in double precision, but changed to 2.22858×10^{-5}, 2.22851×10^{-5}, and then to 2.22568×10^{-5} in the 16, 13 and 8 bit depth fields, respectively. Furthermore, the transformation of data to limited bit depths has an exaggerated effect on the smallest g_{j_i} values. Such values can easily turn into zeros during the transformation, and thus impact the calculation of the partition function. From Eq. (5), it is clear that the partition function is very sensitive to very small values when $q \ll 0$; the slightest changes to these values will cause distinctive alterations to the partition function. The above factors are intertwined and act together to introduce bias in the calculation of the partition function and generalized dimensions as bit depth is reduced.

Multifractal grayscale fields with positive skew appear to be particularly prone to the bit depth effect (see Table 1 and Figs. 3(a)–3(c) and 4(a)–4(c)). This is because of the exceptionally high frequency of very small g_{j_i} values in such fields (Fig. 2(a)). Histograms of the natural grayscale images also exhibited different shapes, with skewness shifting from positive to negative (Fig. 2(d)–2(f)). However, the partition functions and generalized dimensions for these fields were not influenced by the bit depth transformation (see Table 1 and Figs. 3(d)–3(f) and 4(d)–4(f)). This contrasting observation can be explained by the general absence of very small g_{j_i} values, even in those natural grayscale images exhibiting pronounced positive skew (compare Fig. 2(d) with 2(a)).

3.3. Generalized Dimensions Estimated by the Numerical Derivative Method

We have shown that limited bit depths can have a pronounced effect on the calculation of the partition function and generalized dimensions when the linear regression method is employed, even when applied to geometrical multifractal fields. The numerical derivative method proposed by Perfect *et al.*[11] was able to eliminate most of the errors introduced by the normalization process. This method was investigated in the present study to see if it could also reduce the bit depth effect. Figure 5 shows the resulting 1:1 relationship between the analytical generalized dimensions and their numerically derived counterparts for all of the RMG fields regardless of their p value or bit depth when β was set equal to b. The maximum absolute difference between the analytical and the numerically derived estimates of D_q was 9.62×10^{-3}, with a maximum RMSE of 5.80×10^{-3}. The numerical derivative

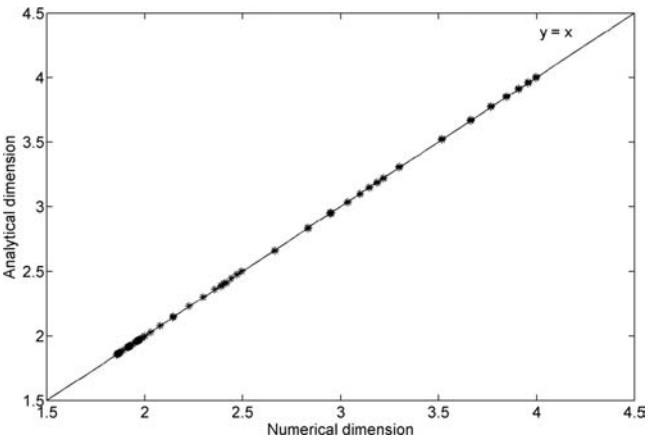

Fig. 5 Relationship between the analytical and the numerically-derived generalized dimensions for all of the RMG fields regardless of p value and bit depth.

method clearly improved the accuracy of the empirical generalized dimensions, and effectively removed their dependence upon bit depth. This is because the bit depth transformation changes the grayscale distribution at small scales, while the numerical derivative method computes the partition function at the largest scales, so it does not "see" any small scale changes.

The numerical derivative method is very effective for analyzing geometrical multifractal fields when β is set equal to b. However, its performance when $\beta \neq b$ is unknown. Also, when using this method on natural grayscale images, there is no underlying b value to guide the choice of β. Moreover, random fluctuations in the linearity of the partition function may influence the numerically derived estimates of D_q since they are based on a narrow range of scales as compared to the linear regression method which covers the entire range of scales. In this case, it is likely that generalized dimensions computed with the numerical derivative method will exhibit a greater dependency on the β value.

To investigate the robustness of the linear regression and numerical derivative methods, both methods were implemented on all of the RMG fields and STS images with $\beta = 2$ and 4, respectively. Compared with the linear form of the partition functions for the double precision RMG fields when $\beta = 4 = b$ (see Fig. 3), the corresponding partition functions when $\beta = 2 \neq b$ showed a characteristic zigzag or saw tooth shape (e.g., Fig. 6). When analyzed with unmatched scale factors, the mass distribution within each box is no longer governed by the truncated binomial distribution and, as a result, nonlinear behavior is manifested in the $\log(\chi(q, \delta))$ versus $\log(\delta)$ relationship.

The numerical derivative method with $\beta = 2 \neq b$ produced erroneous D_q values for the RMG fields because it is based on a particular scale interval and, thus, is particularly sensitive to local changes

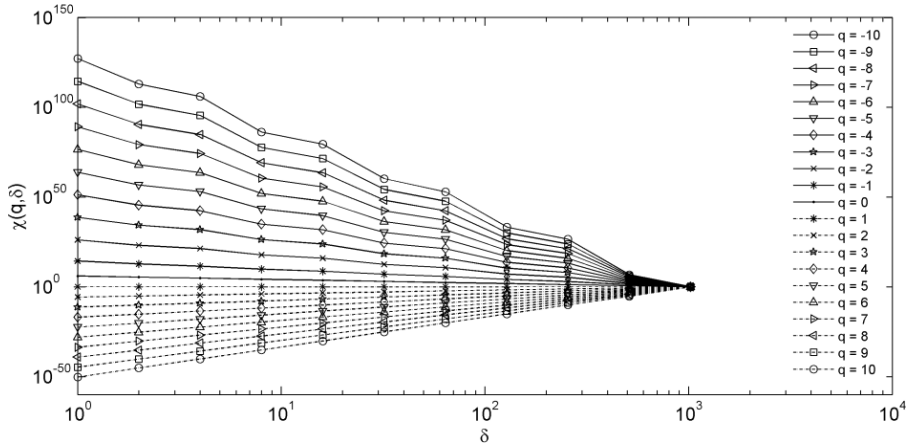

Fig. 6 Partition function for RMG #1 in double precision with $\beta = 2 \neq b$.

Table 3 Statistical Differences Between Generalized Dimensions Estimated Using Different β Values When Analyzing the 13 Bit Depth Grayscale Fields.

Field	Linear Regression Method			Numerical Derivative Method		
	RMSE	Mean % Deviation	Max % Deviation	RMSE	Mean % Deviation	Max % Deviation
RMG#1	0.010	0.004	0.010	2.191	44.78	98.11
RMG#2	0.010	0.004	0.009	1.244	28.74	75.52
RMG#3	0.012	0.004	0.010	0.373	9.855	31.09
STS#1	0.039	0.008	0.026	0.003	0.111	0.351
STS#2	0.041	0.010	0.031	0.068	3.003	6.018
STS#3	0.005	0.001	0.005	0.036	1.318	4.798

Note: RMG = multifractal grayscale field, STS = soil thin section image; root mean square error (RMSE), mean % deviation and maximum (max) % deviation refer to $\frac{D_q(\beta=2)-D_q(\beta=4)}{D_q(\beta=4)}$ for $-10 \leq q \leq 10$.

in slope. RMSE's between the generalized dimensions computed with $\beta = 2$ and 4 ranged from 0.37 to 2.19 for this method (Table 3). The corresponding mean percent deviation ranged from 9.86% to 44.78%, with a maximum percent deviation of 98.10% (Table 3). On the other hand, all of the R^2 values from the linear regression method with $\beta = 2 \neq b$ were > 0.96 (Table 2), despite the saw tooth shape of the partition functions. There were only small differences between the linear regression estimates of D_q for the different β values (Table 2). A statistical summary of these differences is given in Table 3. The RMSE for the linear regression method varied from 0.010 to 0.012, while both the mean and maximum percent deviations were $< 0.01\%$. Similar, albeit less pronounced, trends were observed for the natural grayscale images (Table 3). In this case the poorer performance of the numerical derivative method can be related to random fluctuations or noise in partition functions for the STS images (Fig. 3(d)).

Alternative methods are often tested solely on mathematical examples, where the results can be calculated analytically. However, as our findings emphasize, it is important that experimental data also be considered. While the numerical derivative method eliminated bit depth effects for RMG fields with known b values, it gave invalid results when β was varied. For high p-value geometrical multifractal fields and natural grayscale images which are less sensitive to bit depth effects, we recommend using the linear regression method since it is more robust and the resulting estimates of D_q do not depend upon the choice of β value.

4. CONCLUSIONS

We used random geometrical multifractal fields with different bit depths (i.e., double precision, 16, 13 and 8 bit depths) to evaluate the effect of bit depth on the generalized dimensions estimated by the moment based box counting method. Decreasing bit depth biased the partition function at $q < 0$, and this effect increased as the p value used to generate the fields decreased. The reason was ascribed to the alteration of local mass distributions and the production of zero values by the normalization and bit depth transformation processes. Multifractal fields generated with low p values are more prone to be effected by limited bit depth because of the high frequency of extremely small mass fractions. Unlike the analysis of the multifractal fields, a decrease in bit depth from 13 to 8 bits did not significantly affect the partition functions and estimated generalized dimensions for soil grayscale images.

Generalized dimension estimated by linear regression method were not accurate for the low p value multifractal fields with limited bit depths. The numerical derivative method was implemented as the box size approaches the field size. This method significantly improved the accuracy of the generalized dimensions; the maximum absolute differences between the analytical and the numerically derived estimates of D_q was 9.62×10^{-3}, and the maximum RMSE was 5.80×10^{-3}.

However, the numerical method proved to be less robust when the scale factor of the field was unknown, which is the case for most natural grayscale images. In this situation, the linear regression method was more acceptable, although some deviation was still observed.

ACKNOWLEDGMENTS

This work was supported in part by NKBRSF (2009CB118607) and the National Key Technologies R & D Program during the 11th Five Year Plan Period funded by the Ministry of Agriculture, China (2006BAD15B01).

REFERENCES

1. T. Parrinello and R. A. Vaughan, Multifractal analysis and feature extraction in satellite imagery, *Int. J. Remote Sens.* **23**(9) (2002) 1799–1825.
2. G. D. Tourassi, E. D. Frederick, C. E. Floyd and E. E. Coleman, Multifractal texture analysis of perfusion lung scans as a potential diagnostic tool for acute pulmonary embolism, *Comput. Biol. Med.* **31**(1) (2001) 15–25.
3. A. Dathe, A. M. Tarquis and E. Perrier, Multifractal analysis of the pore-and solid-phases in binary two-dimensional images of natural porous structures, *Geoderma* **134**(3–4) (2006) 318–326.
4. A. N. Posadas, D. Gimenez, R. Quiroz and R. Protz, Multifractal characterization of soil pore systems, *Soil Sci. Soc. Am. J.* **67**(5) (2003) 1361–1369.
5. N. Bird, M. C. Diaz, A. Saa and A. M. Tarquis, Fractal and multifractal analysis of pore-scale images of soil, *J. Hydrol.* **322**(1–4) (2006) 211–219.
6. S. L. Mills, G. C. Lees, C. M. Liauw, R. N. Rothon and S. Lynch, Prediction of mechanical properties following the dispersion assessment of flame retardant filler/polymer composites based on the multifractal analysis of SEM images, *J. Macromol. Sci.* **44**(6) (2005) 1137–1151.

7. S. Balter, Fundamental properties of digital images, *RadioGraphics* **12** (1993) 129–141.
8. H. G. Hentschel and I. Procaccia, The infinite number of generalized dimensions of fractals and strange attractors, *Physica D* **8**(3) (1983) 435–444.
9. L. P. Hansen, Large sample properties of generalized method of moments estimators, *Econometrica* **50**(4) (1982) 1029–1054.
10. D. Veneziano, G. E. Moglen and R. L. Bras, Multifractal analysis: pitfalls of standard procedures and alternatives, *Phys. Rev. E* **52**(2) (1995) 1387–1398.
11. E. Perfect, A. M. Tarquis and N. R. Bird, Accuracy of generalized dimensions estimated from grayscale images using the method of moments, *Fractals* **17**(3) 351–363.
12. G. P. Patil, Maximum likelihood estimation for generalized power series distributions and its application to the truncated binomial distribution, *Biometrika* **49** (1962) 227–237.
13. C. P. Murphy, *Thin Section Preparation of Soils and Sediments* (AB Academic, Berkhampstead, 1986).